Plasmon-Enhanced Fluorescence in Electrospun Nanofibers of Polydiacetylenes Infused with Silver Nanoparticles

Andrew J. Burris and Quan Cheng*
Department of Chemistry, University of California, Riverside, California 92521, USA

*Corresponding author: Quan Cheng, Tel: (951) 827-2702, email: quan.cheng@ucr.edu

Keywords: polydiacetylene, metal-enhanced fluorescence, electrospinning, composite nanofibers

Abstract:

A hybrid computational and experimental approach was employed toward the rational design of a silver nanoparticle (AgNP) / polydiacetylene (PDA) metal-enhanced fluorophore (MEF) ensemble system contained within a polyethylene oxide (PEO) electrospun nanofiber matrix for creation of high-performance sensors. Simulations based on Mie theory and FDTD algorithms were performed to understand and optimize spectral overlap between the AgNP localized surface plasmon resonance and the absorbance and emission spectra of PDA, a supramolecular polymer fluorophore. A series of silver nanoparticles of varied sizes were investigated for fluorescence enhancement capability, and an optimal size of 134 nm in diameter was chosen for synthesis and incorporation into the electrospun nanofibers of a PDA/PEO composite for experimental characterization and confirmation. Results on individual nanofibers indicated a clear metal-enhanced fluorescence effect, and a 4.6–fold enhancement over neat PDA/PEO fluorescent nanofibers was observed. The nanofiber/nanoparticle/MEF ensemble system offers new avenues for generating effective sensing devices with polymeric fluorophores using a straightforward incorporation approach.

Introduction

Metal-enhanced fluorescence (MEF) is a notable strategy for signal amplification in fluorescence-based systems, with applications including single molecule imaging, optoelectronics, and biological and chemical sensors.[1–5] Owing to the coupling of energy between localized surface plasmon resonance (LSPR) of noble metal nanostructures and nearby fluorophores, MEF is known to increase quantum yield and improve the photostability of fluorophores. Effective at distances of roughly 5–90 nm, the MEF technique has been shown to enhance fluorescence signals by just a few percent to several-fold within ensemble systems, and by as much as 400-fold in some single-molecule studies.[6,7]

Polydiacetylenes (PDAs) have been studied extensively as a sensor material, due to a characteristic blue-to-red chromic transformation, accompanied by a fluorescence turn-on event. However, the red-phase of PDA displays weak fluorescence output due to low quantum yield (~0.02), making MEF an attractive technique for PDA signal enhancement.[8–11] A range of studies have explored colorimetric, Raman, nanoelectronics, and photonics strategies with hybrid materials of PDA and noble metal nanostructure materials[12–19]; however, very few literature examples reported MEF on PDA in a sensing setting. There are a few works that have utilized noble metals to amplify the signal of PDA-based sensors, yet their underlying enhancement mechanisms relied on thermochromism or mechanochromism, rather than plasmonic enhancement.[20,21]

Recently, Park and co-workers demonstrated metal-enhanced fluorescence of polydiacetylene-based liposomes using gold nanoparticles.[22] Cui *et al*. synthesized core-shell Ag@PDA nanoparticles that exhibit MEF effect.[23] However, to the best of our knowledge, there

has been no report that explores MEF using PDA-embedded electrospun nanofibers. Nanofiber systems are of particular interest because confinement of an MEF system within nanofibers can improve MEF over that of thin-film systems.[24] Furthermore, when integrated into a sensor, the high specific surface area of nanofibers may improve response time and sensitivity over thin films.

Optimal MEF has been shown to occur when the dipolar LSPR band of AgNP overlaps with the emission spectrum of a fluorophore, or falls within the valley between the absorption and emission bands.[25] Achieving maximal MEF with large polymer fluorophores such as PDAs requires AgNPs of significant size, upwards of 100 nm in diameter. However, established procedures for the synthesis of such large AgNPs were not well-controlled for nanoparticle diameter, thus producing colloids of large size distribution. The introduction of a new synthetic method by Bastús *et al*. enables formation of highly homogeneous AgNP colloids with controlled particle diameters up to 200 nm, making possible the improved tuning of AgNP LSPR spectral overlap with PDA.[26]

In this paper, we investigated AgNP-enhanced fluorescence in PDA / PEO composite electrospun nanofibers for screening of high performing sensors (**Scheme 1**). Mie theory and finite-difference time domain (FDTD) simulations were employed to predict the LSPR wavelength of different sized AgNP colloids, optimize spectral overlap between the AgNP and PDA fluorescence emission, and show feasibility of MEF upon embedment of the ensemble within a nanofiber substrate. AgNPs of optimal diameter were synthesized, capped with a 10 nm polyvinylpyrrolidone (PVP) spacer layer to prevent nanoparticle aggregation while minimizing fluorescence quenching of PDA by the AgNP. Fluorescence of single electrospun nanofibers was

characterized by fluorescence microscopy and the metal-enhanced fluorescence effect was analyzed.

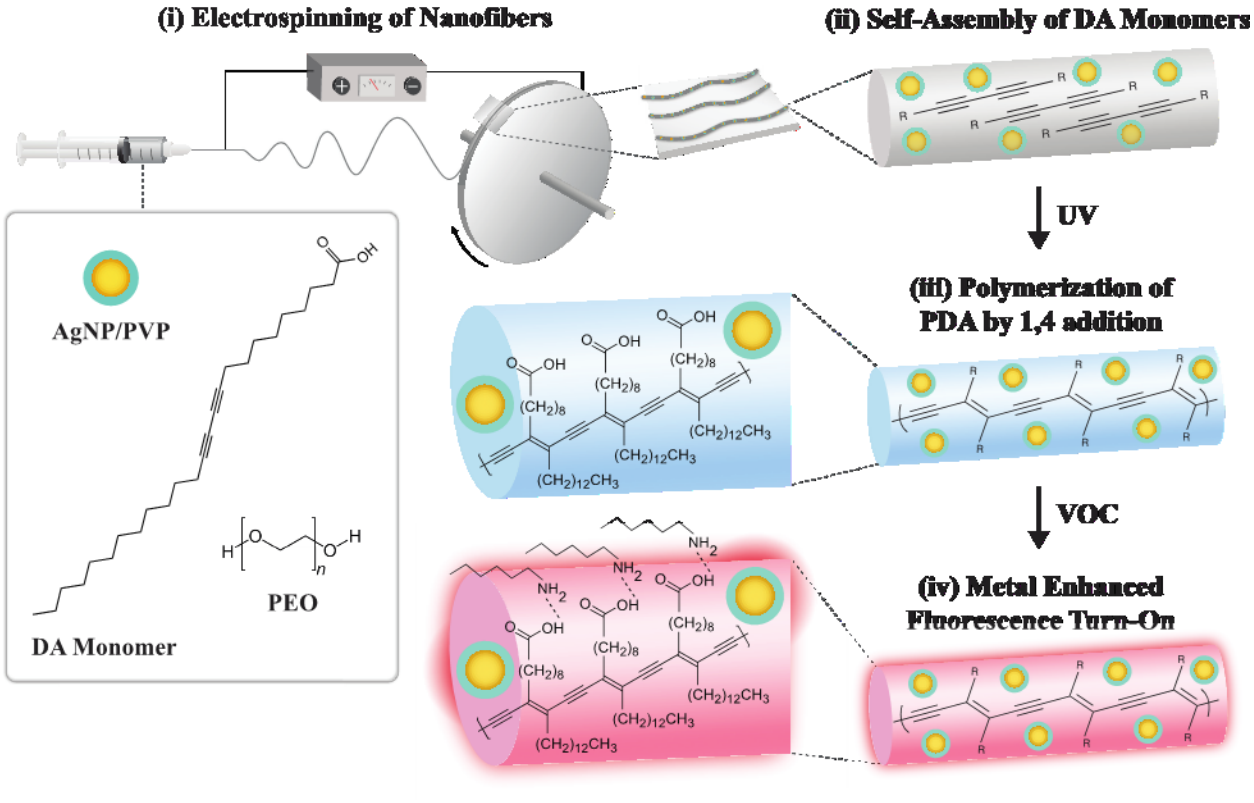

Scheme 1. Fabrication and characterization of metal-enhanced fluorescence sensing of PDA/AgNP/PEO electrospun nanofibers.

Experimental

Mie Theory and FDTD Simulations. Optical cross-sections of AgNP colloids were simulated using Oldenburg's Mie theory calculator, where the absorption and scattering cross sectional areas contribute to the total extinction cross section of the silver nanosphere.[27] Simulations of AgNPs embedded in a nanofiber matrix were conducted using EM Explorer Studio finite-difference time domain (FDTD) software. Metal-enhanced fluorescence (MEF) simulations were performed using Lumerical FDTD software. Lumerical software is a 3D/2D Maxwell's equations solver for nanophotonic devices that facilitates modeling the interaction between a dipole source (fluorophore) and an optical antenna (metal nanosphere).

Materials. All chemicals were used without further purification. The diacetylene monomer, 10,12-pentacosadiynoic acid (PCDA), was purchased from GFS chemicals (Powell, OH). Poly(ethylene oxide) (PEO, M_v = 1,000,000), silver nitrate (99.9999% trace metals basis), trisodium citrate dihydrate (TSC), tannic acid (TA), polyvinylpyrrolidone (PVP10, M_v = 10,000), chloroform, and absolute ethanol were obtained from Sigma-Aldrich (St. Louis, MO). For experiments requiring water, 18 MΩ/cm E-pure water (ddH_2O) was used throughout.

Synthesis of 134 nm Silver Nanoparticles (AgNPs)

AgNPs of 134 nm were synthesized using a seeded growth method reported in the literature.[26] First, AgNP seeds of approximately 15 nm were synthesized by combining 375 mL ddH_2O with 100 mL trisodium citrate (TSC, 25 mM) and 20 mL tannic acid (TA, 2.5 mM) and heated to 90ºC. To the mixture, 5 mL $AgNO_3$ (25 mM) was added, and the solution refluxed for

20 minutes. For each growth step, 100 mL of seed solution was removed and discarded, and a 1.5 mL aliquot was reserved for UV-Vis absorbance characterization. To the remaining 400 mL of seed solution, 85 mL ddH_2O was added, and the temperature brought back to 90ºC. Injections of 2.5 mL TSC (25 mM), 7.5 mL TA (2.5 mM), and 5.0 mL $AgNO_3$ (25 mM) were added, and the solution was refluxed for 20 minutes. The growth step was repeated multiple times, until a 23rd generation was reached, yielding monodisperse Ag nanoparticles of approximately 134 nm in diameter. The resulting citrate-capped Ag nanoparticles were centrifuged twice at 1,500 rpm (180 RCF) to remove residual TA and TSC and washed with a 5 mM polyvinylpyrrolidone (PVP10) solution. The resulting solution was stirred overnight at room temperature to replace the citrate cap with a PVP10 layer of approximately 10 nm. The PVP-capped AgNPs were further purified by centrifugation twice at 180 RCF to remove residual PVP, concentrated 24–fold by washing with a small amount of EtOH.

Fabrication of AgNP / PDA / PEO Nanofibers

Electrospinning solutions were prepared for nanofiber substrates using an ethanol / chloroform solvent system. Two different PCDA monomer-doped solutions were created, each containing 134 nm AgNP or no AgNP (control). A stock solution of PCDA was made by dissolving 25 mg PCDA (0.63% w/v) in 4 mL of a 3:1 EtOH:$CHCl_3$ mixture. The resulting clear pink solution was filtered through a 0.2 µm PTFE syringe filter (Scientific Strategies, Yukon, OK) to remove polymerized PCDA monomers, yielding a clear, colorless solution. To create PCDA-doped solutions, 1.5 mL of AgNP/EtOH colloid was combined with 0.42 mL $CHCl_3$, 80 µL of 0.63% PCDA stock, and 32 mg (1.6 % w/v) poly(ethylene oxide) (PEO) and stirred for 60 minutes in the

dark, resulting in a colorless viscous solution. Control solutions of PCDA-doped systems were prepared using neat EtOH in place of AgNP colloids.

All solutions were prepared fresh and immediately fabricated into nanofibers at room temperature (~25°C) and 42% relative humidity. Electrospun PDA-embedded nanofibers were fabricated by a home-built system as described previously.[28] In brief, the viscous solution was pumped from a 10 mL syringe connected to a 23–gauge blunt tip needle (Braintree Scientific, Inc.) at a rate of 1.0 mL h^{-1} by a syringe pump (KD Scientific, Model 200 series). The application of a high voltage (8 kV) to the metal syringe needle led to generation of nanofibers on the surface of a grounded rotating aluminum disc (20 cm dia., 5 mm wide, 350 rpm) placed 14 cm from the syringe tip. Fiber samples for fluorescence microscopy were collected for 30 seconds on 1 inch cut glass slides which were mounted to the surface of the aluminum disc collector. Fiber samples for electron microscopy were collected for 5 minutes onto conductive carbon tape adhered to aluminum disc collector. All fiber samples were dried overnight in the dark to remove residual solvent. As-spun PCDA nanofibers appeared colorless to the naked eye. Photopolymerization of PCDA monomer-embedded nanofibers was carried out by UV irradiation at 254 nm (1 m W cm^{-2}) for 5 minutes. The nanofibers remained near colorless, due to the small number of fibers collected and relatively low concentration of PDA within the matrix.

Nanoparticle Characterization

AgNPs were characterized using UV-Vis absorbance and nanoparticle tracking analysis (NTA). Nanofibers were characterized using scanning electron microscopy (SEM) and energy-dispersive X-ray spectroscopy (EDX). UV-Vis absorbance measurements were recorded on a

Varian Cary 50 spectrophotometer at room temperature. NTA data were obtained on a Malvern Panalytical NanoSight NS300 (Westborough, MA). SEM images were obtained on a Hitachi TM-4000 scanning electron microscope (Tokyo, Japan). EDX spectra were collected on a Zeiss EVO MA10 scanning electron microscope (Jena, Germany).

VOC Vapor Sensing and Fluorescence Microscopy Measurements

All fluorescence microscopy measurements of the electrospun nanofibers were recorded on a Bioimager inverted epi-fluorescence microscope with mercury illumination (BIM800FLW) at room temperature (~25ºC) equipped with a TRITC filter cube (CHROMA) and a QImaging Retiga 1300 camera. ImageJ software was used for nanofiber diameter measurements and for processing of fluorescence images. PDA-embedded nanofibers were affixed to the underside of a glass petri dish lid and exposed to organic vapors released by a 100 μL droplet of hexylamine liquid for 5 minutes to induce a change from non-fluorescent blue-phase PDA to fluorescent red-phase PDA.

Results and Discussion

Simulations based on Mie Theory and FDTD Method

Figure 1 shows the absorbance spectra of monodisperse silver nanoparticle colloids of varying diameters simulated using Oldenburg's Mie theory software. A characteristic redshift is observed with increasing AgNP diameter. The main peaks, occurring at 460 nm and larger, represent the dipolar LSPR peaks for each colloid, while the secondary peaks appearing at 450 nm

and smaller are multipolar LSPR peaks. Figure 1(b) shows the simulated dipolar SPR peaks overlaid with the absorbance and emission bands of PDA. The 140 nm AgNP exhibits excellent spectral overlap with the PDA emission band and the valley between the PDA absorbance and emission bands. Accordingly, the 140 nm AgNP was selected for further simulation and experimental work.

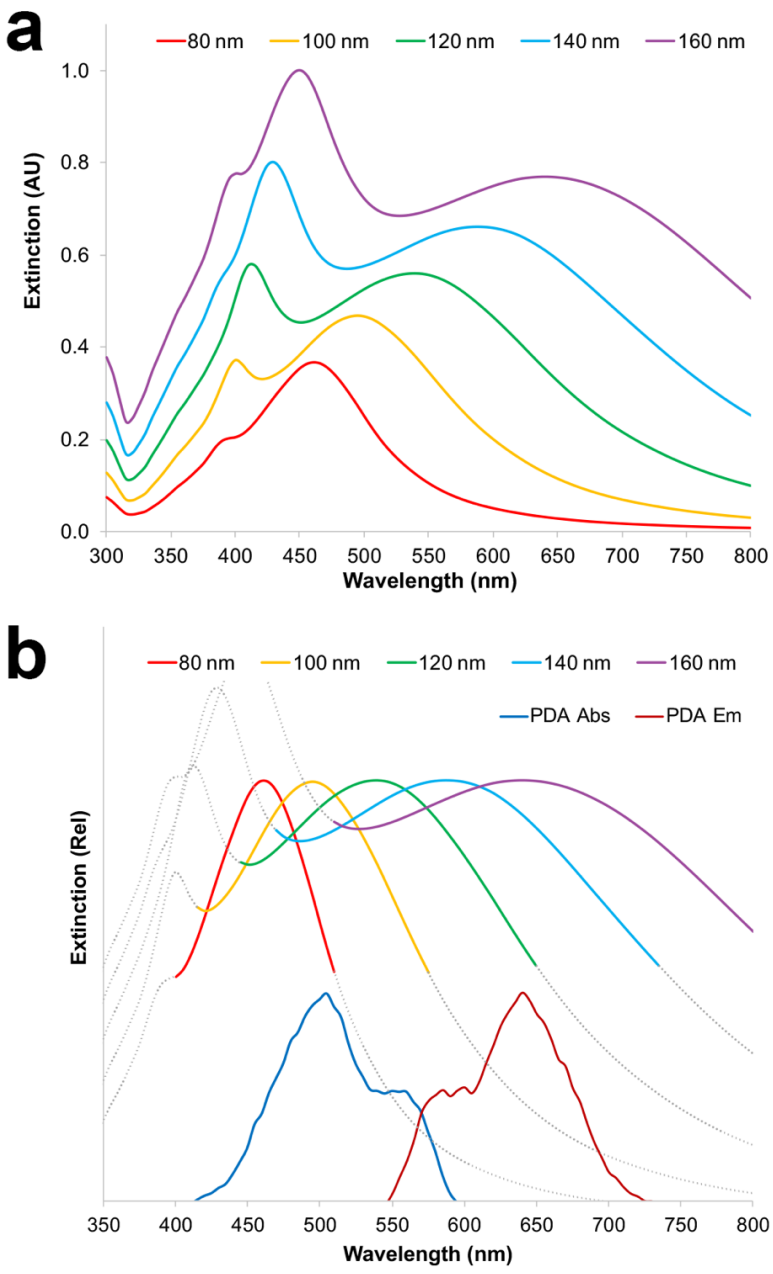

Figure 1: (a) Mie theory simulation for absorbance of AgNPs of diameters from 80–160 nm; (b) spectral overlap of normalized simulated AgNP absorbance and experimentally obtained PDA absorbance and emission spectra.

Next, FDTD simulations were performed using groupings of one, two, three, or four 140 nm AgNPs possessing a 10 nm PVP cap, with a spacing of 10 nm between neighboring nanoparticles (Figure 2). The simulated AgNP systems were irradiated at 492 nm, which is the maximal absorbance for red-phase PDA. The refractive index used for PVP was 1.535, and silver *n* & *k* values were obtained from a data set provided by Jiang, Y. et al., which is an improvement upon the work of Palik and Johnson & Christy.[29] A visual representation of the localized surface plasmon intensity surrounding a single AgNP is shown in 2(a). When multiple AgNPs reside within proximity to one another, plasmon intensity is greatly increased inside of the 10 nm boundaries between silver nanoparticles, as shown in Figure 2(b-d). These so-called hotspots can dramatically increase metal-enhanced fluorescence within the AgNP and PDA ensemble MEF system.

Further FDTD simulations were performed to determine whether embedding AgNPs inside the PEO electrospun nanofiber matrix is detrimental to the plasmonic activity of the AgNPs. Simulations employed a four-nanoparticle cluster of PVP-capped AgNPs placed in different locations within an 800 nm diameter PEO nanofiber placed on a glass slide. A refractive index of 1.454 was used for PEO. The simulation configuration is shown in Figure 3(a), where a PVP-capped AgNP cluster is placed within the center of the nanofiber. The nanofiber, AgNPs, and glass slide are represented by the colors red, purple, and green, respectively. The system was irradiated at 492 nm along the z-axis, opposite the glass slide. The simulation results are shown for various

placements of the nanoparticle cluster within the center of the nanofiber (Fig. 3b), which corresponds to the configuration shown in Figure 3(a), as well as for AgNP placements near the bottom (Fig. 3c), and top (Fig. 3d) of the nanofiber. The results observed in Figure 3(b-d) show visualized local surface plasmon activity is similar to that of Figure 2(d), demonstrating that localized plasmonic activity of the AgNPs appears to be maintained, irrespective of the location of the AgNP cluster within the nanofiber.

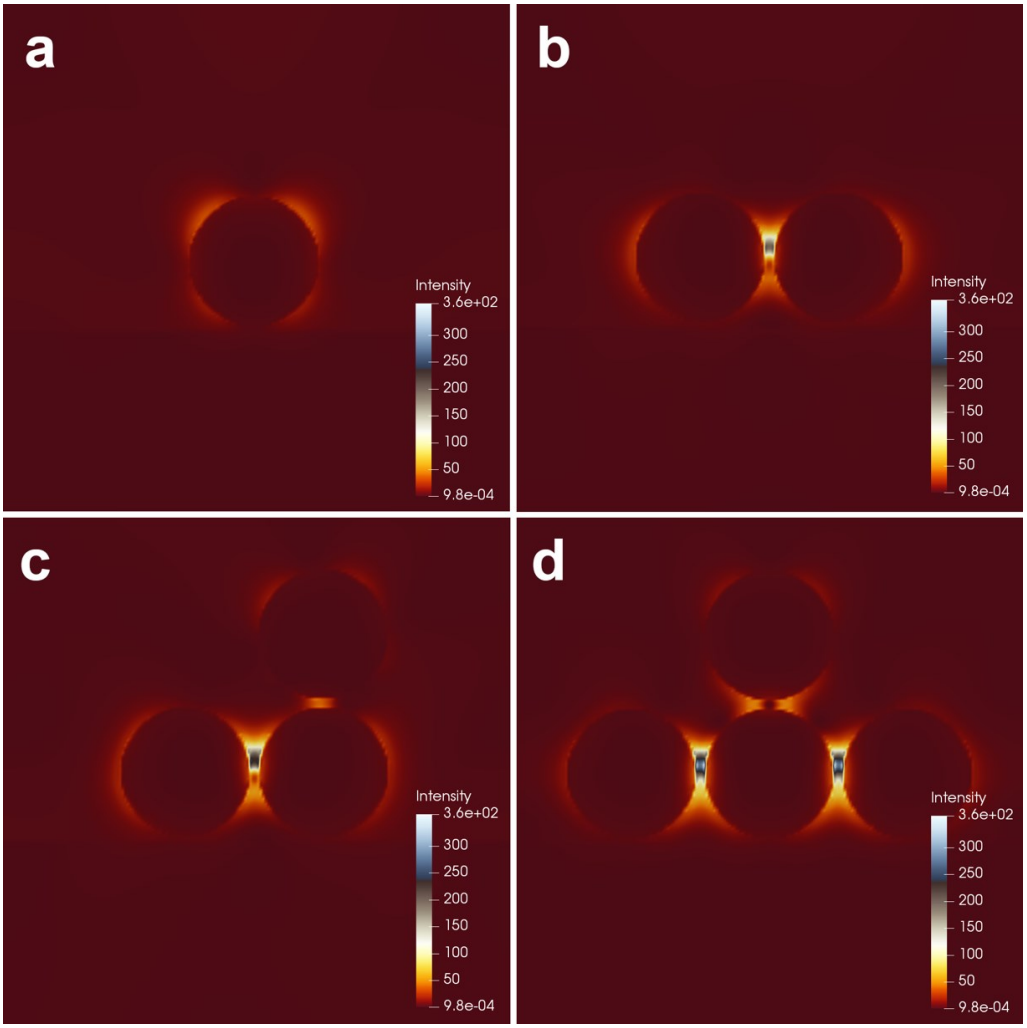

Figure 2. FDTD simulations of localized surface plasmon resonance occurring when (a) one, (b) two, (c), three, or (d) four 140 nm AgNPs with a 10 nm PVP cap are irradiated at 492 nm, the excitation wavelength of PDA.

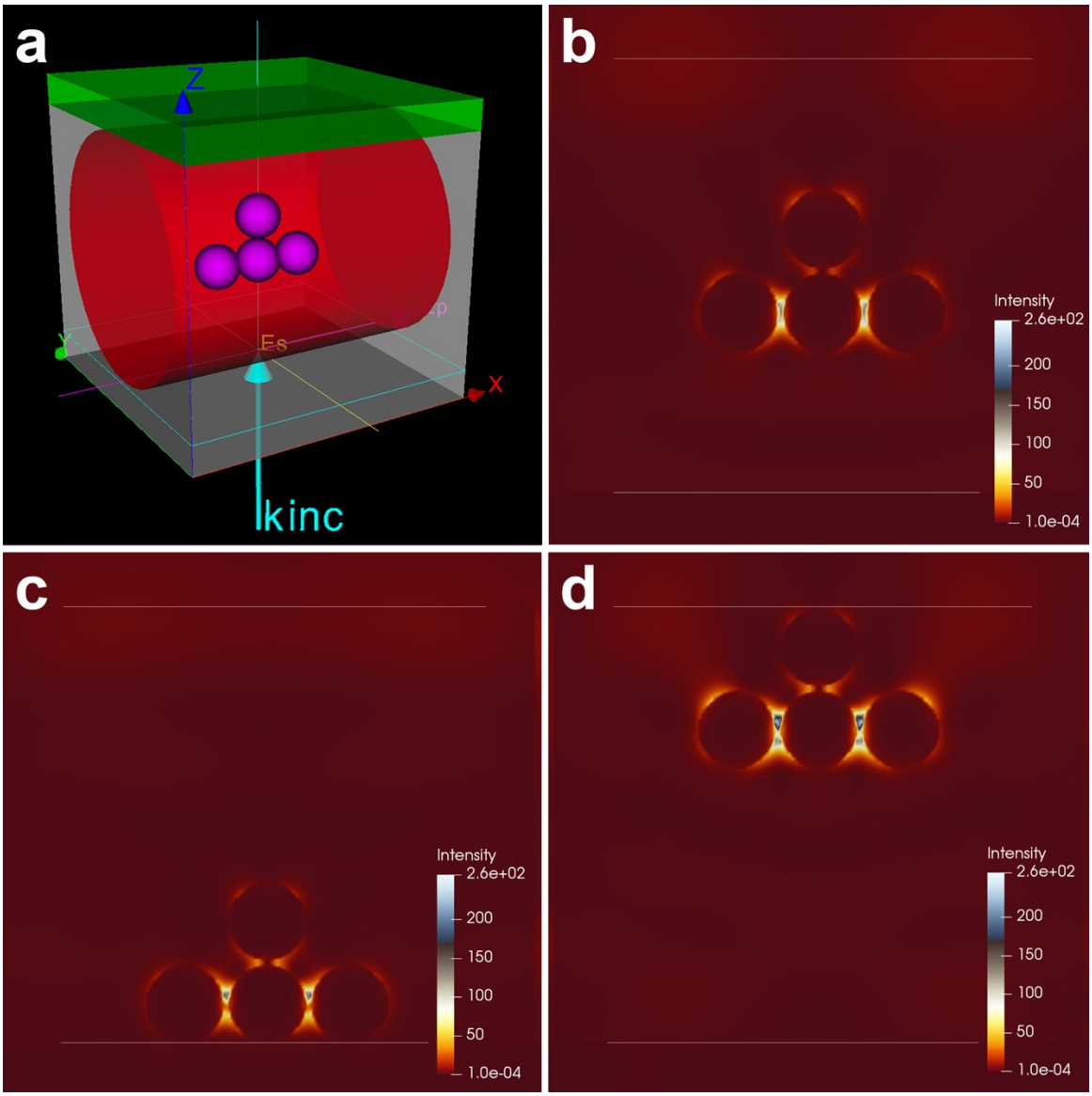

Figure 3: FDTD simulation setup (a) and results (b-d) of localized surface plasmon resonance for a cluster of four 140 nm AgNP with a 10 nm PVP cap is placed in the center (b), bottom (c), or top (d) locations within a PEO nanofiber are irradiated at 492 nm.

The next simulation was performed to investigate the spectral effects of the 10 nm PVP cap added to the 134 nm silver nanoparticle. The 134 nm diameter was selected to maintain consistency with the average size of the experimentally synthesized AgNPs. The purpose of the PVP cap is twofold: 1) to provide protection against nanoparticle aggregation during the

centrifugation-assisted concentration steps, and 2) to serve as a spacer layer, preventing FRET quenching from occurring between the AgNP and the PDA fluorophore. As shown in Figure S1(a-b), the addition of the PVP cap did not induce a significant redshift in the absorbance of the Ag nanoparticle colloid. The result indicates that the PVP-capped AgNP maintains similar spectral overlap with PDA as that of the uncapped AgNP. The redshift observed in the water matrix (Fig. S1a) is more dramatic than that of the PEO matrix (Fig. S1b), presumably due to the larger difference in refractive index (RI) between the water matrix (RI 1.333) and PVP cap (RI 1.535) compared with the PEO nanofiber matrix (RI 1.454) and PVP cap (RI 1.535). In the experimental system, the AgNPs will reside within the PEO nanofiber matrix, where the RI redshift is minimal.

Characterization of 134 nm AgNPs

Based on Mie theory simulation results shown in Figure 1, a target diameter of 140 nm was selected for the experimental silver nanoparticles. AgNP colloids were synthesized via a stepwise seeded growth procedure and characterized by NTA and UV-Vis absorbance techniques. Starting with 12 nm AgNP seeds, a total of 23 synthesis steps were required to obtain the 134 nm AgNPs. Photographs of aliquots from each growth step is shown in Figure S2.

The size of the AgNPs were measured by NTA (Figure 4a), revealing an average diameter of 134 nm, where a near-gaussian size distribution is slightly skewed by AgNPs in the 105-125 nm size range, presumably the result of artifacts from previous growth steps. UV-Vis absorbance spectra (Figure 4b) show a maximum absorbance at approximately 625 nm. The absorbance maximum and peak shape is consistent with values reported in the literature. The dipolar LSPR peak near 625 nm is broad, which is known to occur as AgNP diameter increases, owing to

improved scattering and not due increased size distribution alone.[30] The peak near 450 nm is a result of quadrupolar resonance, a typical feature of Ag nanoparticles with a diameter larger than 80 nm.[31] The shoulder peak near 350 nm is likely due to multipolar resonance, or possibly resulting from the slightly skewed size distribution. Literature values corresponding to the λ_{max} of 625 nm for the colloid suggest an average diameter of 140 nm, consistent with data provided by NTA and absorbance measurements.

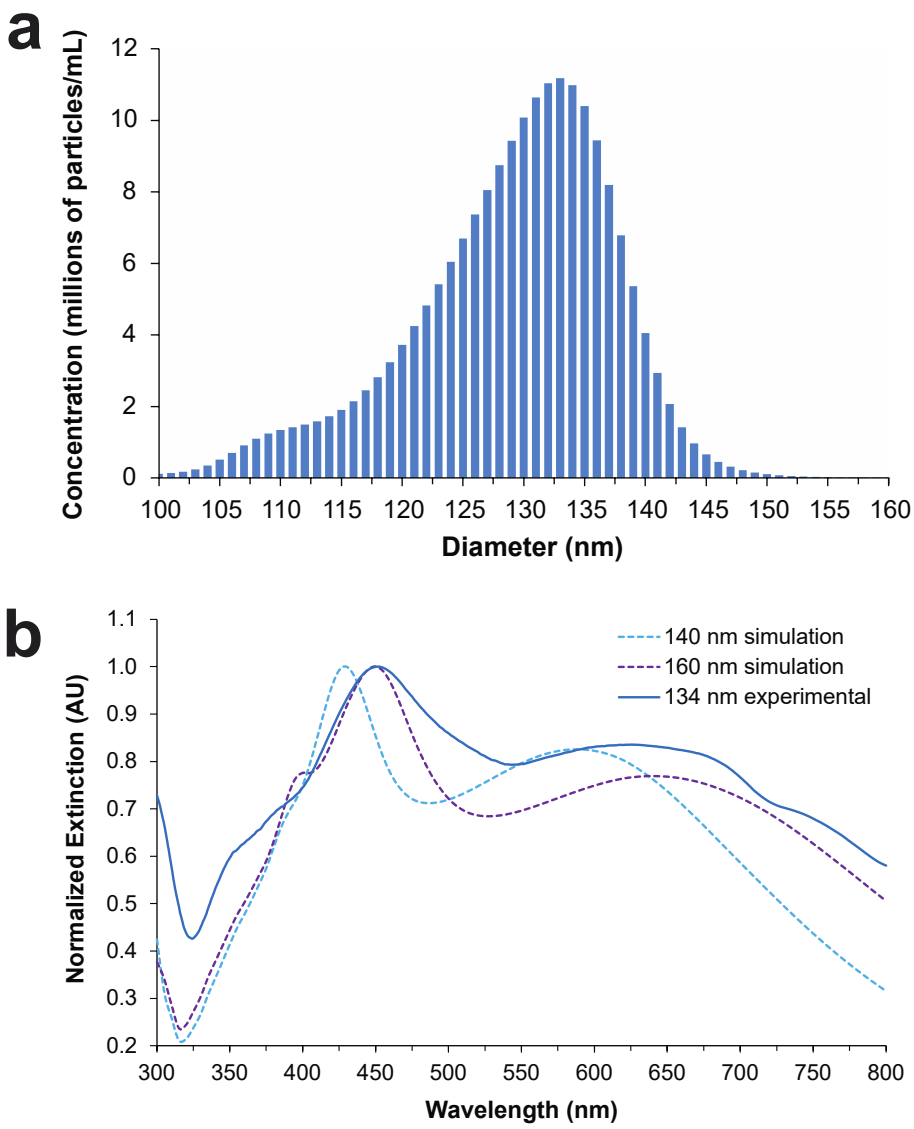

Figure 4: (a) Size distribution of 134 nm AgNPs measured by nanoparticle tracking analysis; (b) UV–Vis absorbance spectra of 134 nm Ag nanospheres shows characteristic quadrupolar and dipolar peaks.

Mie theory simulated absorbance spectra for 140 nm and 160 nm AgNPs are overlaid in Figure 4 along with the absorbance spectrum for the experimental 134 nm AgNPs. The synthesized AgNPs appear to be more consistent with the 160 nm simulation than the 140 nm simulation—this is due to the red shift bias that occurs when measuring the absorbance of an as-synthesized colloid with a gaussian distribution of nanoparticle diameters. When some degree of AgNP colloid polydispersity exists, the largest particles are much more effective at scattering, resulting in a redshift in the overall absorbance peak. In contrast, the simulation data is based on a strictly monodisperse colloid. The redshift effect is especially pronounced in AgNP colloids with larger nanoparticles, where scattering is greatly increased.

The concentration of AgNPs in the colloid solution was measured directly using NTA, yielding 2.2 x 10^{10} AgNPs/mL or 0.30 mg/mL, accounting for a 100-fold dilution. After concentration by centrifugation (24-fold) and a slight dilution (1.3-fold) during electrospinning solution preparation, the estimated concentration of AgNPs present in the nanofiber precursor solution was 4.0 x 10^{11} AgNPs/mL or 5.3 mg/mL. Using the physical properties of the nanofiber constituents (PDA, PEO, and Ag), the estimated concentration of AgNPs in the as-spun, dried electrospun nanofibers was roughly 20% (w/w) or 2.5% (v/v).

Assessment of Simulation-Relevant Properties of PDA Supramolecular Fluorophore

The size of the supramolecular PDA fluorophore was estimated as follows. The PCDA monomer length can be estimated by representing PCDA as a 26-membered linear hydrocarbon,

where a typical carbon-carbon single bond is 154 pm in length, or 126 pm when measured across the longitudinal axis of the hydrocarbon due to the angle of sp^3 C-C bonds. Because a quasi-linear conformation of the PCDA monomer is required for self-assembly with nearby PCDA monomers, the PCDA monomer can be estimated as 3 nm in length. Next, in the direction orthogonal to the monomer chain axis, the size of the polymerized PDA fluorophore can be estimated using values from the literature. The typical PDA supramolecule size is about 30 mer in the solid state, and the repeating unit distance of the main PDA chain is roughly 0.5 nm, irrespective of side chain identity.[32,33] Thus, the PDA supramolecular fluorophore possesses a length of approximately 15 nm. Multiple PDA supramolecules can be held together by attractive forces of π–π stacking, hydrogen bonding, and hydrophobic interactions to form nano- or microcrystals on the order of 30 nm to 1 μm in size, depending on the identity of the pendant side chains, as well as fabrication method and experimental conditions.[34–36] Therefore, based on the size of the PDA supramolecular assemblies and the larger crystals, it is possible that multiple PDA supramolecular polymer fluorophores will surround a single 137 nm AgNP within the MEF range (~ 5-90 nm) of the localized surface plasmons.

Metal-Enhanced Fluorescence (MEF) Simulations

The interaction between fluorophore and AgNP was modeled using Lumerical FDTD metal-enhanced fluorescence solver. Figure 5(a) shows the three-dimensional representation of the simulation configuration containing the antenna (AgNP) and dipole emitter (fluorophore). The radius of the antenna was set to 69.9 nm, corresponding to an AgNP diameter of 140 nm. The Ag material model is based on data from Palik.[37] The distance between AgNP surface and the dipole

emitter was varied from 5–50 nm to simulate different metal-to-fluorophore distances. Dipole orientation was perpendicular, and the measurement wavelength range was 300–800 nm. The FDTD geometry was set to 1 µm, and the mesh accuracy was 3. Mesh override was set to 5 nm, and mesh system x and y spans were set to 250 nm, while the z span was increased above 250 nm until the dipole resided halfway between mesh points. Dipole span was set to 10 nm, structure span to 250 nm, and dipole z span set to match dipole distance from AgNP surface. Simulation time z-geometry was set to 100 nm, while index x and z-span were set to 150 nm, and field profile x- and z-span were 2.1 µm.

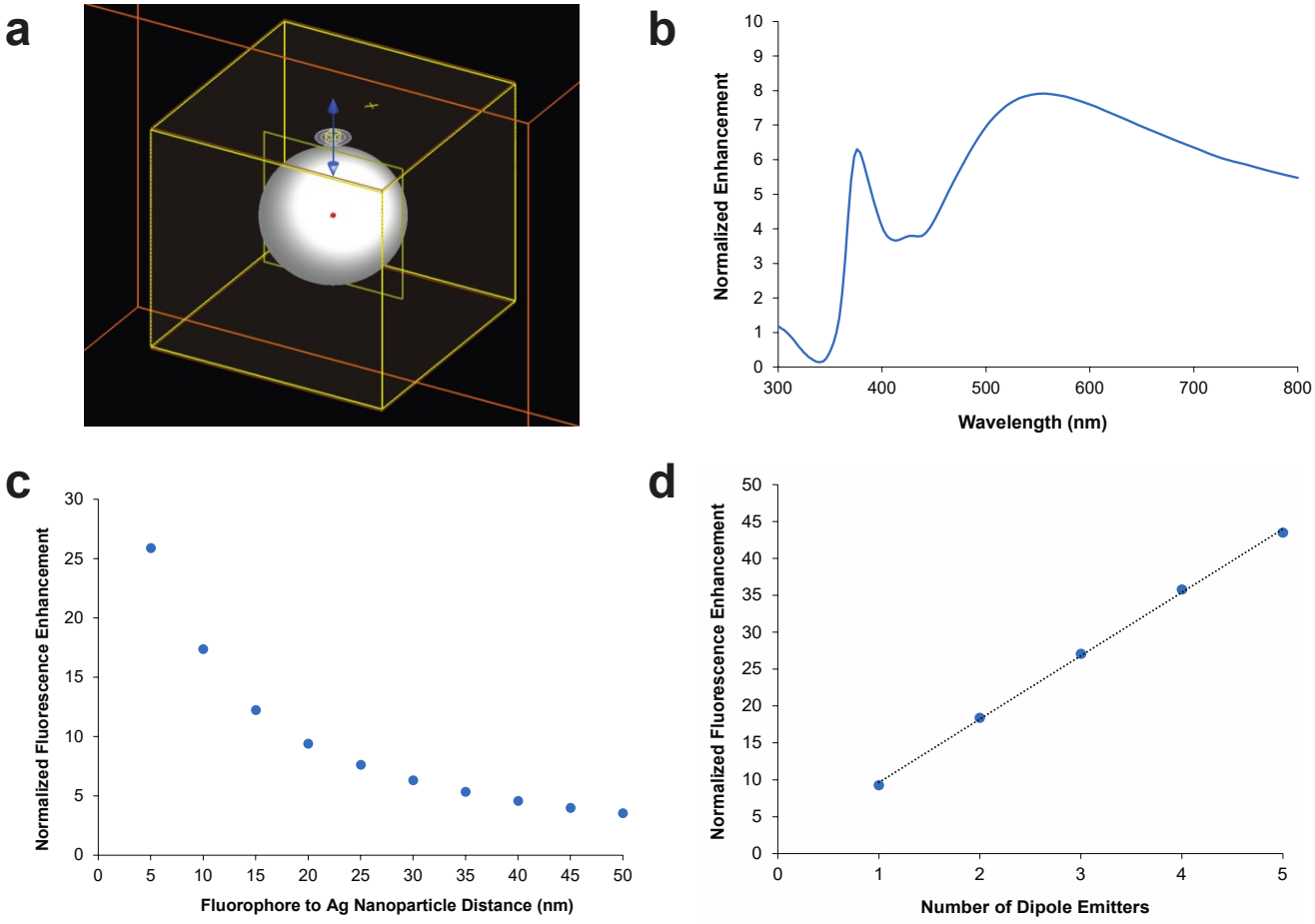

Figure 5. (a) 3-D representation of FDTD simulation configuration modeling interaction between a 140 nm Ag nanoparticle and dipole emitter (fluorophore); FDTD simulation results for (b) varying

fluorescence enhancement of different fluorophore emission wavelengths with a AgNP-to-fluorophore separation distance of 25 nm; (c) fluorescence enhancement of a 600 nm fluorophore at different separation distances; (d) increased fluorescence enhancement when multiple fluorophores reside within 20 nm of a 140 nm AgNP, thereby simulating the interaction of a polymeric fluorophore and a nearby individual silver nanoparticle.

Normalized metal-enhanced fluorescence for a fluorophore modeled as a dipole emitter placed 25 nm away from the surface of a 140 nm silver nanoparticle is shown in Figure 5(b). The increase in fluorescence enhancement for the peak near 570 nm is attributed to the maximal LSPR activity of a 140 nm AgNP. The broadness of the peak is due to the improved scattering of larger silver nanoparticles and confirms that a 140 nm AgNP can support fluorescence enhancement of fluorophores with absorbance and emission bands spanning the 480–700 nm range. The results from multiple simulations are combined in Figure 5(c), where fluorescence enhancement near 600 nm was plotted as fluorophore-to-AgNP separation distance was varied from 5–50 nm. The purpose of this simulation with respect to the PDA fluorophore is to establish that a supramolecular fluorophore (or multiple PDAs), with physical dimensions of roughly 3 nm x 15 nm—larger than that of a typical organic fluorophore molecule—can fully reside within the MEF distance of a 140 nm AgNP. Note that that separation distances smaller than 5 nm were not modeled, given that overlap of the dipole and AgNP simulation geometries would result in simulation errors. However, separation gaps smaller than 5 nm are known to reside within the FRET quenching regime. Furthermore, the presence of a 10 nm PVP cap would most likely preclude any separation gaps smaller than 10 nm from occurring.

Next, the simulation was carried out at a fluorophore-nanoparticle distance of 20 nm, and the number of dipole emitters surrounding the single 140 nm AgNP were increased. Multiple

dipole emitters were employed to roughly model the behavior of a supramolecular fluorophore such as PDA. The separation distance between each dipole emitter was 0.5 nm, which is consistent with the repeating unit distance within PDA chains. The data in Figure 5(d) confirms a linear relationship between enhancement of fluorescence output and the number of dipole emitters, suggesting that metal-enhanced fluorescence of a supramolecular fluorophore is a realistic strategy for signal enhancement.

Characterization of Electrospun Nanofibers and Their Fluorescence Enhancement

Electrospun nanofibers of the AgNP / PDA / PEO composite were then evaluated for metal-enhanced fluorescence by steady-state fluorescence microscopy. SEM images shown in Figure 6 reveal well-defined electrospun nanofibers of (a) AgNP / PDA / PEO and (b) neat PDA / PEO with visibly similar diameters. The AgNP-doped nanofibers shown in Figure 6(a) exhibit a pretzel rod morphology with silver nanoparticles randomly distributed throughout the nanofiber. The EDX spectra in Figure 6(c-d) confirm the presence of silver atoms in the experimental nanofibers, where the control nanofibers consist of carbon and oxygen atoms only. Using SEM images, multiple diameter measurements of the AgNP-doped and neat PDA / PEO nanofibers were made, the resulting histograms shown in Figure S3. The results reveal that the two sets of nanofibers are nearly identical in diameter. The AgNP-doped nanofibers measured an average diameter of 677 ± 17 nm (Figure S3a) while the neat PDA/PEO nanofibers measured 672 ± 18 nm (Figure S3b). Consistency of nanofiber diameter is critical with respect to fluorescence measurements because any differences will affect the amount of PDA present in the fiber, thereby biasing the fluorescence measurements.

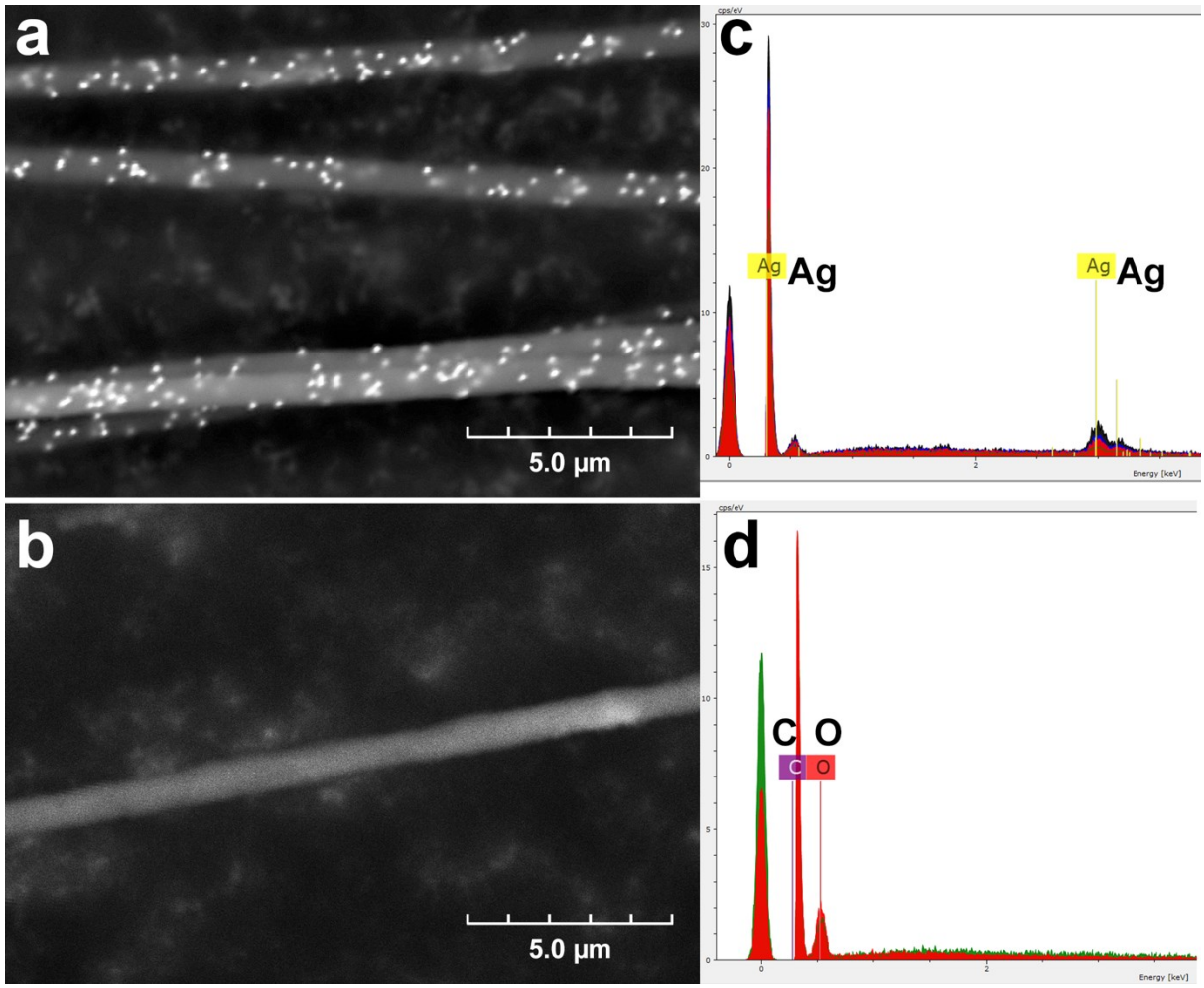

Figure 6. SEM images of (a) AgNP-doped and (b) neat PDA/PEO electrospun nanofibers. EDX spectra of (c) AgNP-doped and (d) neat PDA/PEO nanofibers.

Steady-state fluorescence microscopic images of neat PDA/PEO and AgNP-doped PDA/PEO electrospun nanofibers are shown in Figure 7, where three nanofibers of each variant are shown. A marked increase in fluorescence intensity is clearly observed in Figure 7(c), where the AgNP-doped nanofibers appear much brighter than the neat PDA/PEO nanofibers. Despite an overall smooth, continuous nanofiber morphology evidenced by the SEM images in Figure 6, both the neat and AgNP-doped nanofibers exhibited an inhomogenous distribution of fluorescent PDA supramolecular crystals in Figure 7. Clearly, this breakup of the PDA domains is not caused by

the presence of silver nanoparticles because the neat PDA / PEO nanofibers also display this inhomogeneity. Rather, as PCDA monomers self-assemble within the electrospinning solution—due to PCDA exhibiting higher attractive forces toward neighboring PCDA molecules than it does toward the more polar PEO polymer—PCDA molecules are likely to form domains. This phase separation between the PCDA lipid and the PEO matrix polymer is especially pronounced when PCDA concentration is low, as is the case in this study, where PDA makes up roughly ~1% (w/w) within the PDA / PEO composite. The PDA concentration was relatively low in this study to minimize background fluorescence.

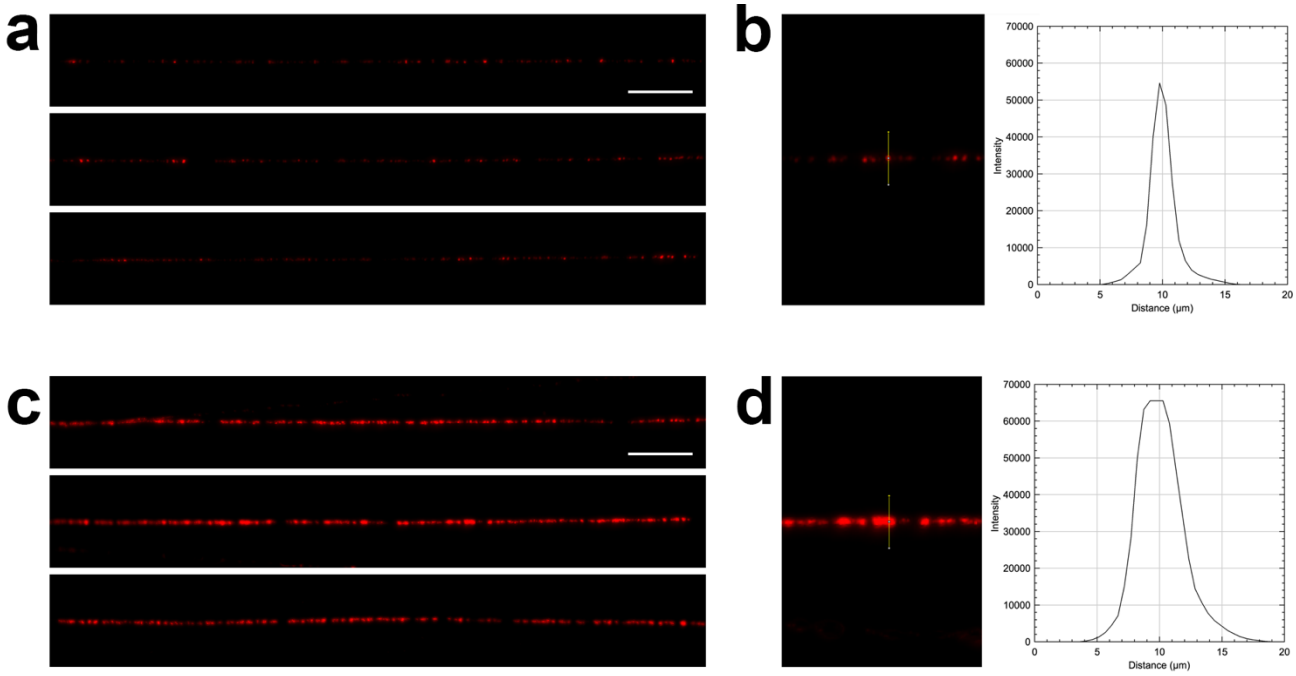

Figure 7. Fluorescence microscopy images of electrospun nanofibers composed of (a) neat PDA/PEO and (c) AgNP-doped PDA/PEO. Scale bars represent 50 micrometers. Surface plots of fluorescence intensities for high intensity spots on electrospun nanofibers composed of (b) neat PDA/PEO and (d) AgNP-doped PDA/PEO.

Analysis of the brightest spots present on the AgNP-doped and neat PDA / PEO fibers reveals amplified fluorescence intensity among the AgNP-doped fibers, shown in the surface profile plots in Figure 7, where a 20 μm long section of fiber was analyzed normal to the fiber. The surface plots reveal an increase in fluorescence output due to the presence of the plasmonic AgNPs. While the surface plots give a good indication of comparative fluorescence, the average intensity output of each fiber was measured, due to the inhomogenous nature of PDA distribution within the nanofibers. In practice, measuring the average intensity is akin to averaging multiple surface plots along the entire length of the nanofiber. A comparison of the average intensity of both AgNP-doped and neat nanofibers reveals an average enhancement factor of 4.6 for the metal-enhanced fluorescent nanofibers (Figure S4). This enhancement of fluorescence signal is attributable to the spectral overlap between the LSPR of AgNP and the absorbance and emission bands of PDA, resulting in the synergistic MEF effect for the PDA / AgNP ensemble system. Furthermore, the presence of the PVP cap on the AgNPs further enhanced the signal in two ways: 1) minimized nanoparticle aggregation, thereby permitting increased concentration of the AgNP colloid during centrifugation (24-fold concentration with PVP cap vs 8-fold without), and 2) suppression of FRET quenching that typically occurs when nanoparticle-to-fluorophore proximity is less than 5 nm.

A comparison this work to other PDA-based MEF studies is summarized in Table 1. With respect to fluorescence enhancement factor (EF), a 4.6-fold enhancement was achieved in this work, while Cui et al. and Park et al. obtained 7-fold and 1.1-fold enhancements, respectively. Comparing to Cui's work, we believe the differences in EF can be explained by the substrate type: the results contained in this work employed an ensemble fluorescence system embedded within a

nanofiber, whereas the work by Cui bound PDA directly to the silver nanoparticles. In our approach, some PDA supramolecules were found to naturally reside beyond the MEF range of the AgNPs. Both works achieved excellent improvement in fluorescence signal, and selection among the two depends on the desired application. Electrospun nanofibers, for example, could be more likely to remain fixed to a solid substrate than would bare nanoparticles. Improvements may be achievable in literature methods by 1) using larger silver nanoparticles to improve spectral overlap, thus increasing MEF, and 2) addition of a spacer material—such as PVP or silica—to the outside of the silver nanoparticle before adhering PDA to the surface.

In contrast with the work by Park, which employed a vesicle platform, this work demonstrated a dramatically larger EF. In addition to substrate differences, Park's work used gold nanoparticles, which are known to exhibit lower plasmonic enhancement than that of silver nanoparticles. In addition, Park and coworkers used 20 nm gold nanoparticles with λ_{max} near 524 nm. Spectral overlap between the gold nanoparticle LSPR and PDA absorbance and emission spectra could be improved by utilizing larger gold nanoparticles of ~80 nm in diameter (λ_{max} near 552 nm). However, the use of larger gold nanoparticles in such a study may interfere with the assembly and/or stability of the PDA vesicles.

Table 1. Comparison of works involving metal-enhanced fluorescence of PDA.

Enhancement Factor (fold)	Nanoparticle Type	Nanoparticle Dia. (nm)	Platform	Reference
7.0	Ag	110	Core-Shell Nanoparticles	Cui [23]
4.6	Ag	137	Electrospun Nanofibers	Present work
1.1	Au	20	Vesicles	Park [22]

Conclusion

While spectral overlap between localized surface plasmons of silver nanoparticles and the absorbance and emission spectra of polydiacetylene can be readily controlled experimentally through trial and error, Mie theory and FDTD calculations provide exceptional tools for the rational design of an electrospun nanofiber-based MEF system. In this work, various simulations were employed to optimize the plasmonic enhancement of a PDA and AgNP ensemble fluorescence system. The computational efforts identified the ideal silver nanoparticle size for maximal spectral overlap with PDA, confirmed that plasmonic activity is maintained when AgNPs reside inside the nanofiber PEO matrix, and showed that a supramolecular fluorophore such as PDA will interact synergistically with a single silver nanoparticle. Electrospun nanofibers of AgNP / PDA / PEO composite were fabricated and evaluated as devices for metal-enhanced fluorescence by interrogating the steady-state fluorescence of individual nanofibers. The AgNP-doped nanofibers exhibited a marked metal-enhanced fluorescence behavior over that of neat PDA / PEO nanofibers. A better understanding on the effect of particle size, concentration, distribution, and embedment on the fluorescence behavior of the conjugated polymer, through both theoretical analysis and experimental exploration, can further improve its performance. Nevertheless, the metal-enhanced fluorescence reported here opens new avenues for advanced PDA-embedded devices, where a dual-mode sensor that takes advantage of both colorimetric and fluorescent qualities of the PDA supramolecule can be employed for the detection of biologically significant targets.

Supporting Information.

The Supporting Information is available free of charge at ACS website.

Mie theory simulation results, silver nanoparticle colloids by a stepwise seeded-growth method, nanofiber diameter measurements, and comparison of fluorescence intensity of different electrospun nanofibers.

Acknowledgements

The authors would like to acknowledge financial support from United States NSF (CHE-2109042). We thank Dr. Wenwan Zhong for the help with the NTA experiments.

References

(1) Badshah, M. A.; Koh, N. Y.; Zia, A. W.; Abbas, N.; Zahra, Z.; Saleem, M. W. Recent Developments in Plasmonic Nanostructures for Metal Enhanced Fluorescence-Based Biosensing. *Nanomaterials* **2020**, *10* (9), 1749.

(2) Lakowicz, J. R.; Ray, K.; Chowdhury, M.; Szmacinski, H.; Fu, Y.; Zhang, J.; Nowaczyk, K. Plasmon-Controlled Fluorescence: A New Paradigm in Fluorescence Spectroscopy. *Analyst* **2008**, *133* (10), 1308–1346.

(3) Kinkhabwala, A.; Yu, Z.; Fan, S.; Avlasevich, Y.; Müllen, K.; Moerner, W. E. Large Single-Molecule Fluorescence Enhancements Produced by a Bowtie Nanoantenna. *Nat. Photonics* **2009**, *3* (11), 654–657.

(4) Hobson, P. A.; Wedge, S.; Wasey, J. A. E.; Sage, I.; Barnes, W. L. Surface Plasmon Mediated Emission from Organic Light-Emitting Diodes. *Adv. Mater.* **2002**, *14* (19), 1393–1396.

(5) Lu, X.; Ye, G.; Punj, D.; Chiechi, R. C.; Orrit, M. Quantum Yield Limits for the Detection of Single-Molecule Fluorescence Enhancement by a Gold Nanorod. *ACS Photonics* **2020**, *7* (9), 2498–2505.

(6) Geddes, C. D.; Lakowicz, J. R. Editorial: Metal-Enhanced Fluorescence. *J. Fluoresc.* **2002**, *12* (2), 121–129.

(7) Ray, K.; Badugu, R.; Szmacinski, H.; Lakowicz, J. R. Several Hundred-Fold Enhanced Fluorescence from Single Fluorophores Assembled on Silver Nanoparticle–Dielectric–Metal Substrate. *Chem. Commun.* **2015**, *51* (81), 15023–15026.

(8) Yoon, B.; Lee, S.; Kim, J. M. Recent Conceptual and Technological Advances in Polydiacetylene-Based Supramolecular Chemosensors. *Chem. Soc. Rev.* **2009**, *38* (7), 1958–1968.

(9) Li, X.; Matthews, S.; Kohli, P. Fluorescence Resonance Energy Transfer in Polydiacetylene Liposomes. *J. Phys. Chem. B* **2008**, *112* (42), 13263–13272.

(10) Fang, F.; Meng, F.; Luo, L. Recent Advances on Polydiacetylene-Based Smart Materials for Biomedical Applications. *Mater. Chem. Front.* **2020**, *4* (4), 1089–1104.

(11) Qian, X.; Städler, B. Recent Developments in Polydiacetylene-Based Sensors. *Chem. Mater.* **2019**, *31* (4), 1196–1222.

(12) Manaka, T.; Yamada, T.; Hoshi, H.; Ishikawa, K.; Takezoe, H. Observation of the Lowest

Ag Excited State Lying in the Optical Gap in Polydiacetylene by Means of Second-Harmonic Generation Spectroscopy. *Synth. Met.* **1998**, *95* (2), 155–158.

(13) Cai, M.; Mowery, M. D.; Pemberton, J. E.; Evans, C. E. Dual-Wavelength Resonance Raman Spectroscopy of Polydiacetylene Monolayers on Au Surfaces. *Appl. Spectrosc.* **2000**, *54* (1), 31–38.

(14) Chen, X.; Zou, G.; Deng, Y.; Zhang, Q. Synthesis and Nonlinear Optical Properties of Nanometer-Size Silver-Coated Polydiacetylene Composite Vesicles. *Nanotechnology* **2008**, *19* (19), 195703.

(15) Saenjaiban, A.; Singtisan, T.; Suppakul, P.; Jantanasakulwong, K.; Punyodom, W.; Rachtanapun, P. Novel Color Change Film as a Time–Temperature Indicator Using Polydiacetylene/Silver Nanoparticles Embedded in Carboxymethyl Cellulose. *Polymers (Basel).* **2020**, *12* (10), 2306.

(16) Zhou, H. S.; Wada, T.; Sasabe, H.; Komiyama, H. Synthesis and Optical Properties of Nanocomposite Silver—Polydiacetylene. *Synth. Met.* **1996**, *81* (2), 129–132.

(17) Bhushan, B.; Kundu, T.; Singh, B. P. Synthesis and Nonlinear Optical Response of Silver Nanoparticles Decorated Polydiacetylene Composite Nanovesicles. *Opt. Commun.* **2014**, *312*, 127–133.

(18) Chen, X.; Tao, J.; Zou, G.; Su, W.; Zhang, Q.; Wang, P. Thermosensitive Silver/Polydiacetylene Nanocrystals with Tunable Nonlinear Optical Properties. *ChemPhysChem* **2010**, *11* (17), 3599–3603.

(19) Liffmann, R.; Homberger, M.; Mennicken, M.; Karthäuser, S.; Simon, U. Polydiacetylene Stabilized Gold Nanoparticles – Extraordinary High Stability and Integration into a Nanoelectrode Device. *RSC Adv.* **2015**, *5* (125), 102981–102992.

(20) Won, S. H.; Sim, S. J. Signal Enhancement of a Micro-Arrayed Polydiacetylene (PDA) Biosensor Using Gold Nanoparticles. *Analyst* **2012**, *137* (5), 1241–1246.

(21) Wu, G.; Mikhailovsky, A.; Khant, H. A.; Fu, C.; Chiu, W.; Zasadzinski, J. A. Remotely Triggered Liposome Release by Near-Infrared Light Absorption via Hollow Gold Nanoshells. *J. Am. Chem. Soc.* **2008**, *130* (26), 8175–8177.

(22) Park, K. H.; Oh, S.; Kim, J.; Yang, S. Y.; An, B. S.; Hwang, D. Y.; Lee, J. H.; Kim, H. S.; Lee, J.; Seo, S. Effect of Surface Charge of Gold Nanoparticles on Fluorescence Amplification of Polydiacetylene-Based Liposomes. *J. Exp. Nanosci.* **2020**, *15* (1), 174–181.

(23) Cui, C.; Kim, S.; Ahn, D. J.; Joo, J.; Lee, G. S.; Park, D. H.; Kim, B. H. Unusual Enhancement of Fluorescence and Raman Scattering of Core-Shell Nanostructure of Polydiacetylene and Ag Nanoparticle. *Synth. Met.* **2018**, *236* (December 2017), 19–23.

(24) Camposeo, A.; Jurga, R.; Moffa, M.; Portone, A.; Cardarelli, F.; Della Sala, F.; Ciracì, C.; Pisignano, D. Nanowire-Intensified Metal-Enhanced Fluorescence in Hybrid Polymer-Plasmonic Electrospun Filaments. *Small* **2018**, *14* (19), 1800187.

(25) Lee, D.; Lee, J.; Song, J.; Jen, M.; Pang, Y. Homogeneous Silver Colloidal Substrates Optimal for Metal-Enhanced Fluorescence. *Phys. Chem. Chem. Phys.* **2019**, *21*, 11599–11607.

(26) Bastús, N. G.; Merkoçi, F.; Piella, J.; Puntes, V. Synthesis of Highly Monodisperse Citrate-Stabilized Silver Nanoparticles of up to 200 Nm: Kinetic Control and Catalytic Properties. *Chem. Mater.* **2014**, *26* (9), 2836–2846.

(27) Oldenburg, S. J. Light scattering from gold nanoshells. Rice Univ., Houston, TX, USA. (2000) 98 pp. https://scholarship.rice.edu/handle/1911/19543.

(28) Burris, A. J.; Tran, K.; Cheng, Q. Tunable Enhancement of a Graphene/Polyaniline/Poly(Ethylene Oxide) Composite Electrospun Nanofiber Gas Sensor. *J. Anal. Test.* **2017**, *1* (2), 12.

(29) Jiang, Y.; Pillai, S.; Green, M. A. Realistic Silver Optical Constants for Plasmonics. *Sci. Rep.* **2016**, *6*, 1–7.

(30) Paramelle, D.; Sadovoy, A.; Gorelik, S.; Free, P.; Hobley, J.; Fernig, D. G. A Rapid Method to Estimate the Concentration of Citrate Capped Silver Nanoparticles from UV-Visible Light Spectra. *Analyst* **2014**, *139* (19), 4855–4861.

(31) Evanoff, D. D. J.; Chumanov, G. Synthesis and Optical Properties of Silver Nanoparticles and Arrays. *Chemphyschem* **2005**, *6* (7), 1221–1231.

(32) Fujita, N.; Sakamoto, Y.; Shirakawa, M.; Ojima, M.; Fujii, A.; Ozaki, M.; Shinkai, S. Polydiacetylene Nanofibers Created in Low-Molecular-Weight Gels by Post Modification: Control of Blue and Red Phases by the Odd-Even Effect in Alkyl Chains. *J. Am. Chem. Soc.* **2007**, *129* (14), 4134–4135.

(33) Kuriyama, K.; Kikuchi, H.; Kajiyama, T. Molecular Packings-Photopolymerization Behavior Relationship of Diacetylene Langmuir-Blodgett Films. *Langmuir* **1996**, *12* (26), 6468–6472.

(34) Nakanishi, H.; Katagi, H. Microcrystals of Polydiacetylene Derivatives and Their Linear

and Nonlinear Optical Properties. *Supramol. Sci.* **1998**, *5* (3–4), 289–295.

(35) Reppy, M. A.; Pindzola, B. A. Biosensing with Polydiacetylene Materials: Structures, Optical Properties and Applications. *Chem. Commun.* **2007**, No. 42, 4317–4338.

(36) Baba, K.; Kasai, H.; Shinohara, Y.; Okada, S.; Oikawa, H.; Matsuda, H.; Nakanishi, H. Chemical Doping into Nanocrystals of Poly(Diacetylene). *Jpn. J. Appl. Phys.* **2008**, *47* (5), 3769–3771.

(37) Palik, E. Handbook of Optical Constants of Solids; Academic Press, 1991; p 1096.

Graphic Content